AIMS Mathematics, 10(11): 28034–28058.
DOI:10.3934/math.20251232
Received: 23 September 2025
Revised: 29 October 2025
Accepted: 03 November 2025
Published: 28 November 2025

https://www.aimspress.com/journal/Math

Research article

Efficient Laplace-based decomposition and iteration techniques for the fractional GHS coupled KdV system with Atangana-Baleanu derivative

Mofida Zaki[1], M. Abdelgaber[1,*], Hoda F. Ahmed[2] and W. A. Hashem[2,3]

[1] Department of Mathematics, College of Science and Arts, Najran University, Najran 66445, Saudi Arabia

[2] Mathematics Department, Faculty of Science, Minia University, Minia, Egypt

[3] Faculty of Computer Science, Nahda University, Beni Suef, Egypt

* **Correspondence:** Email: maebrahem@nu.edu.sa.

Abstract: This study explored efficient solution strategies for the fractional generalized Hirota-Satsuma (GHS) coupled KdV system, which serves as a fundamental model for describing nonlinear wave interactions across various branches of physics and engineering, including nonlinear dispersive-wave phenomena in plasma and optical fibers. In particular, attention was focused on the GHS-KdV system governed by the Atangana-Baleanu Caputo fractional derivative (AB-CFD), which effectively captures the distinctive memory and hereditary features of complex materials and wave propagation phenomena. We presented two advanced Laplace-based methods: the Laplace Adomian decomposition method (LADM) and Laplace variational iteration method (LVIM) that effectively capture the system's nonlinear dynamics and memory effects without requiring linearization or perturbation. Numerical validation confirmed the methods' accuracy through excellent agreement with exact solutions, demonstrating systematic convergence as additional terms were included and complete recovery of classical solutions when fractional orders approached integer values. The mathematical consistency of both approaches is verified through comprehensive error analysis. These results establish LADM and LVIM as efficient computational tools for nonlinear fractional PDEs, particularly valuable for modeling wave propagation in complex media and other systems exhibiting hereditary properties. The methods offer significant advantages in handling the nonlocal characteristics inherent to fractional systems while maintaining computational efficiency.

Keywords: Atangana-Baleanu Caputo fractional derivative; generalized Hirota-Satsuma coupled KdV system; Laplace Adomian decomposition method; Laplace varitional iteration method
Mathematics Subject Classification: 26A33, 65D12, 91G20

1. Introduction

Fractional calculus, an extension of classical calculus that generalizes derivatives and integrals to non-integer orders [1], has become a crucial mathematical framework for modeling complex systems with inherent memory and hereditary effects. Unlike traditional calculus, which is restricted to integer-order derivatives, fractional calculus enables the study of phenomena such as viscoelasticity, anomalous diffusion, and complex wave dynamics. These capabilities make it particularly effective for modeling systems exhibiting long-range dependencies. Consequently, fractional calculus has found applications in diverse fields, including fluid dynamics [2], plasma physics [3], and nonlinear optics [4], where classical models often fail to capture the underlying system behavior [5].

The generalized Hirota-Satsuma (GHS) coupled Korteweg-de Vries (KdV) system, introduced in [6], is widely recognized as a fundamental model for describing nonlinear wave interactions. This system arises in several real-world physical and engineering scenarios. In fluid dynamics, it models the evolution of shallow water waves in channels, harbors, and coastal regions, which is essential for hydraulic and coastal engineering applications. In plasma physics, it describes ion-acoustic plasma waves, which play a crucial role in controlled fusion devices and space plasma environments. In nonlinear optics, the system captures the propagation of nonlinear optical pulses in fiber optics and photonic media.

Over the years, numerous studies have proposed various approaches to solve the GHS-KdV system, ranging from numerical techniques to semi-analytical methods [7–12]. While these methods have provided valuable insights, incorporating fractional derivatives into the model significantly increases its complexity, necessitating advanced solution strategies capable of capturing both the memory and nonlinear characteristics of the system.

The adoption of fractional derivatives, particularly the Atangana-Baleanu derivative [13], represents a notable advancement in the mathematical modeling of complex dynamical systems. The AB-CFD incorporates a nonlocal Mittag-Leffler (ML) kernel that is non-singular at the origin and exhibits an intermediate memory decay, slower than exponential but faster than a power law. This memory structure has been shown to better reflect the relaxation and dispersive dynamics of many complex wave media. In contrast to Caputo and Riemann-Liouville operators, whose singular kernels enforce strong power-law memory, and the Caputo-Fabrizio operator with its rapidly fading exponential behavior, the AB-CFD introduces a smooth hereditary law without nonphysical singularities. As a result, it offers an enhanced and physically grounded framework for modeling nonlinear wave propagation and transport phenomena where history-dependent effects are essential [14–17]. Despite these advantages, the analytical and numerical treatment of fractional differential equations involving the AB-CFD operator remains challenging due to the strong nonlinearity, non-locality, and memory dependence inherent in such models, especially for systems like the fractional GHS-KdV equation. For the GHS coupled KdV system, where nonlinear dispersive waves interact through multifield dynamics, variations in memory strength can significantly influence transient propagation characteristics. The AB-CFD formulation offers a flexible framework that:

- captures non-singular fading memory in time-fractional models.
- preserves physical nonlocality through the ML kernel.
- recovers the classical GHS-KdV dynamics as the fractional order tends to one.

Classical models often fail to fully account for memory and nonlocal effects inherent in these systems, whereas fractional derivatives, particularly those with non-singular kernels, offer a more realistic and flexible framework for describing wave evolution and dissipation in such complex media. In Table 1, we provide a comparison of representative time-derivative models used for KdV-type equations, highlighting the kernel behavior, memory-decay characteristics, and short-time regularity. Our AB-based model occupies a distinct position within this comparison.

Table 1. Representative time-derivative models for KdV systems (qualitative comparison).

Time derivative	Kernel $K(t)$	Short-time behavior	Memory decay	Notes
Classical ($\theta = 1$)	$\delta(t)$	Markovian	None	Recovers standard GHS-KdV
Caputo/RL for $\alpha \in (0,1)$	$K(t) \sim t^{-\theta}$ (singular)	Power-law singular	Power-law tail	Strong long memory; classical fractional models
Caputo-Fabrizio	Exponential (non-singular)	Finite at 0	Exponential	Short memory; fast forgetting
Atangana-Baleanu (AB-CFD)	Mittag-Leffler (non-singular, nonlocal)	Finite at 0	ML/stretched-exp type	Distinct transient dynamics; kernel used in this work

Given these analytical challenges, several advanced solution techniques have been developed to address the intricacies introduced by fractional derivatives. For example, Rania Saadeh [18] applied the Laplace residual power series method (LRPSM) to solve the nonlinear time-fractional GHS-KdV equation using Caputo fractional derivatives. In [19], a fractional complex transform and a modified Adomian decomposition method were employed. Similarly, the q-homotopy analysis transform method (q-HATM) was utilized in [20] to study the nonlinear Caputo fractional GHS-KdV. Heydari [21] employed discrete Legendre polynomials with a collocation scheme, while the authors in [22] applied a pseudo-spectral method to address the time-fractional GHS-KdV system. Recent work [23] introduced two novel semi-analytical techniques for solving the fractional GHS-KdV system: the Aboodh residual power series method (ARPSM) and the Aboodh transform iteration method (ATIM). Additionally, the spatio-temporal fractal fractional coupled Hirota system was numerically solved in [24].

Since traditional methods often perform poorly when handling non-singular memory laws. We explore the specific impact of the AB-CFD kernel on solution behavior by embedding it within Laplace-enhanced LADM and LVIM algorithms. These techniques are then employed to compute accurate and efficient solutions of the following fractional GHS-KdV system.

$$\begin{aligned}
{}^{ABC}_{0}\mathcal{D}_t^{\theta}\phi(x,t) &= \rho_1\,\phi_{xxx}(x,t) - \rho_2\,\phi(x,t)\,\phi_x(x,t) + \rho_3\left(\psi(x,t)\,\varphi(x,t)\right)_x,\\
{}^{ABC}_{0}\mathcal{D}_t^{\theta}\psi(x,t) &= -\sigma_1\,\psi_{xxx}(x,t) + \sigma_2\,\phi(x,t)\,\psi_x(x,t),\\
{}^{ABC}_{0}\mathcal{D}_t^{\theta}\varphi(x,t) &= -\delta_1\,\varphi_{xxx}(x,t) + \delta_2\,\phi(x,t)\,\varphi_x(x,t),
\end{aligned} \tag{1.1}$$

along the initial conditions (ICs):

$$\phi(x,0) = \phi_0(x), \qquad \psi(x,0) = \psi_0(x), \qquad \varphi(x,0) = \varphi_0(x). \tag{1.2}$$

Here, $\phi(x,t)$, $\psi(x,t)$, *and* $\varphi(x,t)$ are unknown functions represent interacting wave fields, $(x,t) \in [A,B] \times [0,L]$, $0 < \theta \leq 1$, the coefficients $\rho_1, \rho_2, \rho_3, \sigma_1, \sigma_2, \delta_1$ and δ_2 are non-negative numbers determining coupling strengths and ${}^{ABC}_{0}\mathcal{D}_t^{\theta}$ is the time AB-CFD.

The LADM integrates the Laplace transform with the Adomian decomposition method, simplifying fractional derivatives into algebraic terms and decomposing solutions into rapidly convergent series. This approach eliminates the need for linearization or perturbation, making it particularly suitable for complex fractional systems such as the GHS-KdV. The effectiveness of the LADM in handling a wide class of differential equations has been demonstrated in several studies; see, for example, [25–27]. The convergence of both the ADM and LADM has been established by various authors for different classes of differential equations involving diverse types of fractional derivatives; see [28–30].

The variational iteration method (VIM) is an iterative approach that constructs correction functionals to approximate solutions. By incorporating the Laplace transform, the VIM simplifies the treatment of complex initial and boundary conditions, thereby improving accuracy. This method effectively integrates memory effects from fractional derivatives, enhancing its applicability to fractional GHS-KdV systems with the AB-CFD. Due to its effectiveness, the LVIM has become a popular choice among researchers seeking semi-analytical solutions for various types of fractional differential equations (FDEs) involving different kinds of fractional derivatives; relevant studies include [26, 27, 31, 32]. The LVIM facilitates rapid convergence and yields progressively more accurate approximations of the exact solutions [33, 34].

Although several methods have been developed for fractional KdV-type equations, incorporating the AB-CFD operator introduces unique analytical and computational challenges due to its non-singular Mittag-Leffler kernel. To address these, we propose Laplace-based decomposition frameworks (LADM and LVIM) tailored to the AB-CFD operator. These hybrid semi-analytical schemes yield rapidly convergent solutions without linearization or discretization, while preserving the physical integrity and computational efficiency of the fractional model.

The proposed LADM and LVIM offer distinct advantages:

- Efficiency and Simplicity: Both methods transform the fractional GHS-KdV system into simpler forms, providing accurate solutions without requiring extensive computational resources.
- Robustness: By leveraging the Laplace transform, these methods effectively handle the nonlinearity and memory effects introduced by the AB-CFD.
- Convergence and Accuracy: The LADM and LVIM exhibit rapid convergence to solutions, achieving high accuracy as validated through comparisons with exact results.
- Wide Applicability: These methods are not only effective for the fractional GHS-KdV system but are also applicable to a broad class of nonlinear fractional differential equations across various scientific and engineering fields.

The novelty of this study is threefold: (i) it presents the first application of the LADM and LVIM to the fractional GHS-KdV system involving the Atangana-Baleanu derivative, (ii) it provides a systematic convergence assessment, and (iii) it offers a comprehensive comparison with recent numerical techniques. Extensive numerical experiments and graphical analyses confirm the superior

accuracy, stability, and efficiency of the proposed methods, positioning them as powerful and reliable tools for solving complex fractional systems.

The paper proceeds as follows: Section 2 introduces the mathematical basic definitions, including the AB-CFD and related essential concepts. Section 3 details the implementation of the LADM and LVIM for solving the fractional GHS-KdV system. Numerical results and analyses are presented in Sections 4 and 5, respectively. The concluding remarks and future research directions are discussed in Section 6.

2. Basic definitions

In this section, we present some fundamental definitions and essential results related to the AB-CFD.

Definition 1. [14] The two-parameter Mittag-Leffler function is defined as

$$E_{\alpha,\beta}(t) = \sum_{k=0}^{\infty} \frac{t^k}{\Gamma(\alpha k + \beta)} \qquad \alpha, \beta \in \mathbb{R}^+, t \in \mathbb{C},$$

which is a generalization of the one-parameter Mittag-Leffler function ($E_\alpha(t) = E_{\alpha,1}(t)$), and the latter is a generalization of the exponential function e^t.

Definition 2. Let $\mathcal{F}(x,t) \in \mathcal{H}^1(a,b)$, $b > a$ *and* $\mathcal{F}(x,t)$ differentiable and let $\theta \in (0,1]$. The AB-CFD is defined as:

$${}^{ABC}_{0}\mathcal{D}_t^{\theta}\mathcal{F}(x,t) = \frac{\mathcal{M}(\theta)}{1-\theta}\int_0^t \frac{\partial \mathcal{F}(x,s)}{\partial s} E_\theta\Big(\frac{-\theta\,(t-s)^\theta}{1-\theta}\Big)ds, \tag{2.1}$$

where $\mathcal{M}(\theta) = 1 - \theta + \frac{\theta}{\Gamma(\theta)}$, $\mathcal{M}(0) = \mathcal{M}(1) = 1$, and $E_\theta\Big(\frac{-\theta\,(t-s)^\theta}{1-\theta}\Big)$ denotes the Mittag-Leffler function of one parameter. For more details and properties of the AB-CFD, refer to [31, 35, 36].

Definition 3. For a piecewise continuous function $u(\xi,t)$ of exponential order σ_0, i.e., there exist constants $M > 0$ and $\sigma_0 \in \mathbb{R}$ such that $|u(\xi,t)| \leqslant Me^{\sigma_0 t}, \quad t \geqslant 0$.

The Laplace transform (LT) with respect to the temporal variable t exists and is given by:

$$\mathcal{L}_t u(\xi,t) = \mathcal{U}(\xi,s) = \int_0^{\infty} u(\xi,\tau)e^{-s\tau}d\tau, \quad s \geq 0, \tag{2.2}$$

and its inverse is given by

$$u(\xi,t) = \mathcal{L}_t^{-1}[\mathcal{U}(\xi,s)] = \int_{c-i\infty}^{c+i\infty} \mathcal{U}(\xi,s)e^{s\tau}ds, \quad c = Re(s). \tag{2.3}$$

Definition 4. The LT of the AB-CFD is defined as [31],

$$\mathcal{L}_t[{}^{ABC}_{\theta}\mathcal{D}_t^{\theta} f(x,t)](s) = \frac{M(\theta)}{1-\theta}\left(\frac{\mathcal{F}(x,s)s^\theta - s^{\theta-1}f(x,0)}{s^\theta + \frac{\theta}{1-\theta}}\right). \tag{2.4}$$

3. Analysis of the proposed methods

3.1. Laplace Adomian decomposition method

In the following, we will summarize the procedure steps of applying the LADM to the fractional GHS coupled KdV system Eq (1.1).

- First, applying the Laplace transform to Eq (1.1) followed by its inverse gives

$$\begin{aligned}
\phi(x,t) &= \phi(x,0) + \mathcal{L}_t^{-1}\left[\varpi(\theta)\mathcal{L}_t\left[\rho_1\,\phi_{xxx}(x,t) - \rho_2\,\mathcal{A}_1(\phi,\phi) + \rho_3(\mathcal{A}_2(\psi,\varphi) + \mathcal{A}_3(\psi,\varphi))\right]\right],\\
\psi(x,t) &= \psi(x,0) + \mathcal{L}_t^{-1}\left[\varpi(\theta)\mathcal{L}_t\left[-\sigma_1\,\psi_{xxx}(x,t) + \sigma_2\,\mathcal{B}(\phi,\psi)\right]\right],\\
\varphi(x,t) &= \varphi(x,0) + \mathcal{L}_t^{-1}\left[\varpi(\theta)\mathcal{L}_t\left[-\delta_1\,\varphi_{xxx}(x,t) + \delta_2\,\mathcal{H}(\phi,\varphi)\right]\right].
\end{aligned} \tag{3.1}$$

  Here $\varpi(\theta) = \frac{\theta + s^{\theta}(1-\theta)}{s^{\theta}M(\theta)}$, $\mathcal{A}_1 = \phi(x,t)\phi_x(x,t)$, $\mathcal{A}_2 = \psi_x(x,t)\varphi(x,t)$, $\mathcal{A}_3 = \psi(x,t)\varphi_x(x,t)$, $\mathcal{B} = \phi(x,t)\psi_x(x,t)$, *and* $\mathcal{H} = \phi(x,t)\varphi_x(x,t)$.
- In the LADM, the solutions $\phi(x,t)$, $\psi(x,t)$, and $\varphi(x,t)$ are expressed as convergent infinite series as:

$$\phi(x,t) = \sum_{n=0}^{\infty}\phi_n(x,t), \qquad \psi(x,t) = \sum_{n=0}^{\infty}\psi_n(x,t) \quad \text{and} \quad \varphi(x,t) = \sum_{n=0}^{\infty}\varphi_n(x,t). \tag{3.2}$$

  The nonlinear components $\mathcal{A}_1$, $\mathcal{A}_2$, $\mathcal{A}_3$, $\mathcal{B}$, and $\mathcal{H}$ are expanded by an infinite series of the Adomian polynomials as

$$\mathcal{A}_1 = \sum_{n=0}^{\infty}\Xi_n, \quad \mathcal{A}_2 = \sum_{n=0}^{\infty}P_n, \quad \mathcal{A}_3 = \sum_{n=0}^{\infty}K_n, \quad \mathcal{B} = \sum_{n=0}^{\infty}\Upsilon_n, \quad \mathcal{H} = \sum_{n=0}^{\infty}\Omega_n, \tag{3.3}$$

  where

$$\begin{aligned}
\Xi_n &= \frac{1}{n!}\Big[\frac{d^n}{d\lambda^n}\Big[\mathcal{A}_1(\sum_{k=0}^{\infty}\lambda^k\phi_k)\Big]\Big]_{\lambda=0} = \frac{1}{n!}\Big[\frac{d^n}{d\lambda^n}\Big[(\sum_{k=0}^{\infty}\lambda^k\phi_k)(D_x(\sum_{k=0}^{\infty}\lambda^k\phi_k))\Big]\Big]_{\lambda=0},\\
P_n &= \frac{1}{n!}\Big[\frac{d^n}{d\lambda^n}\Big[\mathcal{A}_2(\sum_{k=0}^{\infty}\lambda^k\psi_k, \sum_{k=0}^{\infty}\lambda^k\varphi_k)\Big]\Big]_{\lambda=0} = \frac{1}{n!}\Big[\frac{d^n}{d\lambda^n}\Big[(D_x(\sum_{k=0}^{\infty}\lambda^k\psi_k))(\sum_{k=0}^{\infty}\lambda^k\varphi_k)\Big]\Big]_{\lambda=0},\\
K_n &= \frac{1}{n!}\Big[\frac{d^n}{d\lambda^n}\Big[\mathcal{A}_3(\sum_{k=0}^{\infty}\lambda^k\psi_k, \sum_{k=0}^{\infty}\lambda^k\varphi_k)\Big]\Big]_{\lambda=0} = \frac{1}{n!}\Big[\frac{d^n}{d\lambda^n}\Big[(\sum_{k=0}^{\infty}\lambda^k\psi_k)(D_x(\sum_{k=0}^{\infty}\lambda^k\varphi_k))\Big]\Big]_{\lambda=0},\\
\Upsilon_n &= \frac{1}{n!}\Big[\frac{d^n}{d\lambda^n}\Big[\mathcal{B}(\sum_{k=0}^{\infty}\lambda^k\phi_k, \sum_{k=0}^{\infty}\lambda^k\psi_k)\Big]\Big]_{\lambda=0} = \frac{1}{n!}\Big[\frac{d^n}{d\lambda^n}\Big[(\sum_{k=0}^{\infty}\lambda^k\phi_k)(D_x(\sum_{k=0}^{\infty}\lambda^k\psi_k))\Big]\Big]_{\lambda=0},\\
\Omega_n &= \frac{1}{n!}\Big[\frac{d^n}{d\lambda^n}\Big[\mathcal{H}(\sum_{k=0}^{\infty}\lambda^k\phi_k, \sum_{k=0}^{\infty}\lambda^k\varphi_k)\Big]\Big]_{\lambda=0} = \frac{1}{n!}\Big[\frac{d^n}{d\lambda^n}\Big[(\sum_{k=0}^{\infty}\lambda^k\phi_k)(D_x(\sum_{k=0}^{\infty}\lambda^k\varphi_k))\Big]\Big]_{\lambda=0}.
\end{aligned} \tag{3.4}$$

- The Adomian polynomials (3.4) can be systematically computed. Below are the first few components:

$$\begin{aligned}
&\Xi_0 = \phi_0 D_x\phi_0, \quad \Xi_1 = \phi_0 D_x\phi_1 + \phi_1 D_x\phi_0, \quad \Xi_2 = \phi_0 D_x\phi_2 + \phi_1 D_x\phi_1 + \phi_2 D_x\phi_0, \ \cdots\\
&P_0 = \varphi_0 D_x\psi_0, \quad P_1 = \varphi_1 D_x\psi_0 + \varphi_0 D_x\psi_1, \quad P_2 = \varphi_2 D_x\psi_0 + \varphi_1 D_x\psi_1 + \varphi_0 D_x\psi_2, \ \cdots\\
&K_0 = \psi_0 D_x\varphi_0, \quad K_1 = \psi_1 D_x\varphi_0 + \psi_0 D_x\varphi_1, \quad K_2 = \psi_2 D_x\varphi_0 + \psi_1 D_x\varphi_1 + \psi_0 D_x\varphi_2, \ \cdots\\
&\Upsilon_0 = \phi_0 D_x\psi_0, \quad \Upsilon_1 = \phi_1 D_x\psi_0 + \phi_0 D_x\psi_1, \quad \Upsilon_2 = \phi_2 D_x\psi_0 + \phi_1 D_x\psi_1 + \phi_0 D_x\psi_2, \ \cdots\\
&\Omega_0 = \phi_0 D_x\varphi_0, \quad \Omega_1 = \phi_1 D_x\varphi_0 + \phi_0 D_x\varphi_1, \quad \Omega_2 = \phi_2 D_x\varphi_0 + \phi_1 D_x\varphi_1 + \phi_0 D_x\varphi_2, \ \cdots
\end{aligned}$$

- Inserting Eqs (3.2) and (3.3) into Eq (3.1) yields

$$\begin{aligned}
\sum_{n=0}^{\infty}\phi_n(x,t) &= \phi_0 + \mathcal{L}_t^{-1}\Big[\varpi(\theta)\,\mathcal{L}_t\Big[\rho_1\sum_{n=0}^{\infty}(\phi_n)_{xxx} \\
&\qquad - \rho_2\sum_{n=0}^{\infty}(\mathcal{A}_1)_n + \rho_3\sum_{n=0}^{\infty}(\mathcal{A}_2)_n + \rho_3\sum_{n=0}^{\infty}(\mathcal{A}_3)_n\Big]\Big], \\
\sum_{n=0}^{\infty}\psi_n(x,t) &= \psi_0 + \mathcal{L}_t^{-1}\left[\varpi(\theta)\mathcal{L}_t\left[-\sigma_1\sum_{n=0}^{\infty}(\psi_n)_{xxx} + \sigma_2\sum_{n=0}^{\infty}\mathcal{B}_n\right]\right], \\
\sum_{n=0}^{\infty}\varphi_n(x,t) &= \varphi_0 + \mathcal{L}_t^{-1}\left[\varpi(\theta)\,\mathcal{L}_t\left[-\delta_1\sum_{n=0}^{\infty}(\varphi_n)_{xxx} + \delta_2\sum_{n=0}^{\infty}\mathcal{H}_n\right]\right].
\end{aligned} \tag{3.5}$$

- By using the linearity property of the LT, the subsequent recursive formulas are attained:

$$\phi_0 = \phi(x,0), \qquad \psi_0 = \psi(x,0), \qquad \text{and} \qquad \varphi_0 = \varphi(x,0). \tag{3.6}$$

$$\begin{aligned}
\phi_1(x,t) &= \mathcal{L}_t^{-1}\left[\varpi(\theta)\mathcal{L}_t\left[\rho_1\,(\phi_0)_{xxx} - \rho_2\,(\mathcal{A}_1)_0 + \rho_3(\mathcal{A}_2)_0 + \rho_3(\mathcal{A}_3)_0\right]\right], \\
\psi_1(x,t) &= \mathcal{L}_t^{-1}\left[\varpi(\theta)\,\mathcal{L}_t\left[-\sigma_1\,(\psi_0)_{xxx}(x,t) + \sigma_2\,\mathcal{B}_0\right]\right], \\
\varphi_1(x,t) &= \mathcal{L}_t^{-1}\left[\varpi(\theta)\,\mathcal{L}_t\left[-\delta_1\,(\varphi_0)_{xxx} + \delta_2\,\mathcal{H}_0\right]\right].
\end{aligned} \tag{3.7}$$

In overall, for $\kappa \geq 1$, we have

$$\begin{aligned}
\phi_{\kappa+1}(x,t) &= \mathcal{L}_t^{-1}\left[\varpi(\theta)\mathcal{L}_t\left[\rho_1\,(\phi_\kappa)_{xxx} - \rho_2\,(\mathcal{A}_1)_\kappa + \rho_3(\mathcal{A}_2)_\kappa + \rho_3(\mathcal{A}_3)_\kappa\right]\right], \\
\psi_{\kappa+1}(x,t) &= \mathcal{L}_t^{-1}\left[\varpi(\theta)\,\mathcal{L}_t\left[-\sigma_1\,(\psi_\kappa)_{xxx} + \sigma_2\,\mathcal{B}_\kappa\right]\right], \\
\varphi_{\kappa+1}(x,t) &= \mathcal{L}_t^{-1}\left[\varpi(\theta)\,\mathcal{L}_t\left[-\delta_1\,(\varphi_\kappa)_{xxx} + \delta_2\,\mathcal{H}_\kappa\right]\right].
\end{aligned} \tag{3.8}$$

- The practical solution will be the κ-term approximations

$$\phi(x,t) \simeq \sum_{n=0}^{\kappa}\phi_n(x,t), \qquad \psi(x,t) \simeq \sum_{n=0}^{\kappa}\psi_n(x,t), \quad \text{and} \quad \varphi(x,t) \simeq \sum_{n=0}^{\kappa}\varphi_n(x,t). \tag{3.9}$$

- The precise solution will be

$$\begin{aligned}
&\phi(x,t) = Lim_{\kappa\to\infty}\sum_{n=0}^{\kappa}\phi_n(x,t), \;\; \psi(x,t) = lim_{\kappa\to\infty}\sum_{n=0}^{\kappa}\psi_n(x,t), \\
&\text{and} \;\; \varphi(x,t) = lim_{\kappa\mapsto\infty}\sum_{n=0}^{\kappa}\varphi_n(x,t).
\end{aligned} \tag{3.10}$$

3.2. Laplace variational iteration method

Consider fractional GHS-KdV system (1.1) defined with the initial conditions in Eq (1.2). The primary steps involved in applying the LVIM can be outlined as follows:

- By taking the Laplace transform of the entire system, we obtain

$$\begin{aligned}
&\frac{M(\theta)}{s^{\theta}(1-\theta)+\theta}\left[s^{\theta}\mathcal{L}_t\phi(x,t)-s^{\theta-1}\,\phi(x,0)\right]-\mathcal{L}_t[\rho_1\,\phi_{xxx}(x,t)-\rho_2\,\phi(x,t)\,\phi_x(x,t)\\
&\qquad+\rho_3\left(\psi(x,t)\,\varphi(x,t)\right)_x]=0,\\
&\frac{M(\theta)}{s^{\theta}(1-\theta)+\theta}\left[s^{\theta}\mathcal{L}_t\psi(x,t)-s^{\theta-1}\,\psi(x,0)\right]-\mathcal{L}_t\left[-\sigma_1\,\psi_{xxx}(x,t)+\sigma_2\,\phi(x,t)\,\psi_x(x,t)\right]=0,\\
&\frac{M(\theta)}{s^{\theta}(1-\theta)+\theta}\left[s^{\theta}\mathcal{L}_t\varphi(x,t)-s^{\theta-1}\,\varphi(x,0)\right]-\mathcal{L}_t\left[-\delta_1\,\varphi_{xxx}(x,t)+\delta_2\,\phi(x,t)\,\varphi_x(x,t)\right]=0.
\end{aligned}\tag{3.11}$$

Let $\mathcal{L}_t\phi(x,t)=\bar{\phi}(x,s)$, $\mathcal{L}_t\psi(x,t)=\bar{\psi}(x,s)$, $\mathcal{L}_t\varphi(x,t)=\bar{\varphi}(x,s)$.

- The iterative formula is formulated as

$$\begin{aligned}
\bar{\phi}_{\kappa+1}(x,s)&=\bar{\phi}_{\kappa}(x,s)+\Lambda_1(s)\Bigg[\frac{M(\theta)}{s^{\theta}(1-\theta)+\theta}\Big(s^{\theta}\bar{\phi}(x,s)-s^{\theta-1}\phi(x,0)\Big)\\
&\qquad-\mathcal{L}_t\Big[\rho_1\phi_{xxx}(x,t)-\rho_2\phi(x,t)\phi_x(x,t)+\rho_3\big(\psi(x,t)\varphi(x,t)\big)_x\Big]\Bigg],\\
\bar{\psi}_{\kappa+1}(x,s)&=\bar{\psi}_{\kappa}(x,s)+\Lambda_2(s)\Bigg[\frac{M(\theta)}{s^{\theta}(1-\theta)+\theta}\Big(s^{\theta}\bar{\psi}(x,s)-s^{\theta-1}\psi(x,0)\Big)\\
&\qquad-\mathcal{L}_t\big[-\sigma_1\psi_{xxx}(x,t)+\sigma_2\phi(x,t)\psi_x(x,t)\big]\Bigg],\\
\bar{\varphi}_{\kappa+1}(x,s)&=\bar{\varphi}_{\kappa}(x,s)+\Lambda_3(s)\Bigg[\frac{M(\theta)}{s^{\theta}(1-\theta)+\theta}\Big(s^{\theta}\bar{\varphi}(x,s)-s^{\theta-1}\varphi(x,0)\Big)\\
&\qquad-\mathcal{L}_t\big[-\delta_1\varphi_{xxx}(x,t)+\delta_2\phi(x,t)\varphi_x(x,t)\big]\Bigg],
\end{aligned}\tag{3.12}$$

where $\Lambda_1(s)$, $\Lambda_2(s)$ *and* $\Lambda_3(s)$ represent the Lagrange multipliers. Set $\frac{\delta\bar{\phi}_{\kappa+1}(x,s)}{\delta\bar{\phi}_{\kappa}(x,s)}=0$, $\frac{\delta\bar{\psi}_{\kappa+1}(x,s)}{\delta\bar{\psi}_{\kappa}(x,s)}=0$, and $\frac{\delta\bar{\varphi}_{\kappa+1}(x,s)}{\delta\bar{\varphi}_{\kappa}(x,s)}=0$, consider the terms $\mathcal{L}_t\left(\rho_1\,\phi_{xxx}(x,t)-\rho_2\,\phi(x,t)\,\phi_x(x,t)+\rho_3\,\left(\psi(x,t)\,\varphi(x,t)\right)_x\right)$, $\mathcal{L}_t\left(-\sigma_1\,\psi_{xxx}(x,t)+\sigma_2\,\phi(x,t)\,\psi_x(x,t)\right)$, and $\mathcal{L}_t\left(-\delta_1\,\varphi_{xxx}(x,t)+\delta_2\,\phi(x,t)\,\varphi_x(x,t)\right)$ as restricted terms and we get

$$\begin{aligned}
1+\frac{M(\theta)s^{\theta}}{s^{\theta}(1-\theta)+\theta}\,\Lambda_1(s)&=0,\\
1+\frac{M(\theta)s^{\theta}}{s^{\theta}(1-\theta)+\theta}\,\Lambda_2(s)&=0,\\
1+\frac{M(\theta)s^{\theta}}{s^{\theta}(1-\theta)+\theta}\,\Lambda_3(s)&=0.
\end{aligned}\tag{3.13}$$

So

$$\Lambda_1(s)=\Lambda_2(s)=\Lambda_3(s)=-\frac{s^{\theta}(1-\theta)+\theta}{s^{\theta}M(\theta)}=-\varpi(\theta).\tag{3.14}$$

- Using the inverse Laplace transform, we arrive at

$$\begin{aligned}
\phi_{\kappa+1}(x,t) &= \phi(x,0) + \mathcal{L}_t^{-1}[\varpi(\theta)\mathcal{L}_t[\rho_1\,(\phi_\kappa)_{xxx}(x,t) - \rho_2\,\phi_\kappa(x,t)\,(\phi_\kappa)_x(x,t) \\
&\quad + \rho_3\,\,(\psi_\kappa(x,t)\,\varphi_\kappa(x,t))_x\,]], \\
\psi_{k+1}(x,t) &= \psi(x,0) + \mathcal{L}_t^{-1}\left[\varpi(\theta)\mathcal{L}_t\left[-\sigma_1\,(\psi_\kappa)_{xxx}(x,t) + \sigma_2\,\phi_\kappa(x,t)\,(\psi_\kappa)_x(x,t)\right]\right], \\
\varphi_{\kappa+1}(x,t) &= \varphi(x,0) + \mathcal{L}_t^{-1}\left[\varpi(\theta)\mathcal{L}_t\left[-\delta_1\,(\varphi_\kappa)_{xxx}(x,t) + \delta_2\,\phi_\kappa(x,t)\,(\varphi_\kappa)_x(x,t)\right]\right],
\end{aligned} \tag{3.15}$$

  using the starting iteration

$$\phi_0(x,t) = \phi(x,0),\;\; \psi_0(x,t) = \psi(x,0),\;\; \varphi_0(x,t) = \varphi(x,0). \tag{3.16}$$

- The exact solution will be

$$\phi(x,t) = lim_{\kappa\longrightarrow\infty}\phi_\kappa(x,t),\;\; \psi(x,t) = lim_{\kappa\longrightarrow\infty}\psi_\kappa(x,t),\;\; \varphi(x,t) = lim_{\kappa\longrightarrow\infty}\varphi_\kappa(x,t). \tag{3.17}$$

4. Numerical studies

We will examine the fractional GHS coupled KdV system represented by Eq (1.1) with the given coefficients, $(\rho_1,\rho_2,\rho_3,\sigma_1,\sigma_2,\delta_1,\delta_2) = (0.5,3,3,1,3,1,3)$ ensuring consistency across the analysis, under two specified initial conditions:

4.1. First kind initial condition

At first, consider the fractional GHS-KdV system Eq (1.1) under the following condition:

$$\begin{aligned}
\phi(x,0) &= \frac{\gamma-2k^2}{3} - 2k^2 tanh^2(kx), \\
\psi(x,0) &= \frac{-4k^2c_0(\gamma+k^2)}{3c_1^2} + \frac{4k^2(\gamma+k^2)}{3c_1} tanh(kx), \\
\varphi(x,0) &= c_0 + c_1 tanh(kx).
\end{aligned} \tag{4.1}$$

It is worth noting that the exact solution of the GHS-KdV system Eq (1.1) at $\theta = 1$ under the initial condition Eq (4.1) is provided in [37] as

$$\begin{aligned}
\phi(x,t) &= \frac{\gamma-2k^2}{3} + 2k^2 tanh^2(k(x+\gamma t)), \\
\psi(x,t) &= \frac{4k^2c_0(\gamma+k^2)}{3c_1^2} + \frac{4k^2(\gamma+k^2)}{3c_1} tanh(k(x+\gamma t)), \\
\psi(x,t) &= c_0 + c_1 tanh(k(x+\gamma t)).
\end{aligned} \tag{4.2}$$

Solution using the LADM

By following the procedure outlined in the previous section, the first few terms of the solution obtained using the LADM are expressed as

$$\begin{aligned}
\phi_0(x,t) &= \frac{\gamma-2k^2}{3} - 2k^2 tanh^2(kx), \\
\psi_0(x,t) &= \frac{-4k^2c_0(\gamma+k^2)}{3c_1^2} + \frac{4k^2(\gamma+k^2)}{3c_1} tanh(kx), \\
\varphi_0(x,t) &= c_0 + c_1 tanh(kx),
\end{aligned} \tag{4.3}$$

and

$$\begin{aligned}
\phi_1(x,t) &= \frac{\gamma k^3 \Gamma(\theta)\tanh(kx)\mathrm{sech}^2(kx)\left((4.\theta-4)\Gamma(\theta+1)-4\theta t^{\theta}\right)}{((\theta-1)\Gamma(\theta)-\theta)\Gamma(\theta+1)},\\
\psi_1(x,t) &= \frac{4\gamma k^3\left(\gamma+k^2\right)\mathrm{sech}^2(kx)\left(-\theta\Gamma(\theta)+\Gamma(\theta)+t^{\theta}\right)}{3c_1(\theta+\theta(-\Gamma(\theta))+\Gamma(\theta))},\\
\varphi_1(x,t) &= \frac{\gamma c_1 k\mathrm{sech}^2(kx)\left(-\theta\Gamma(\theta)+\Gamma(\theta)+t^{\theta}\right)}{\theta+\theta(-\Gamma(\theta))+\Gamma(\theta)}.
\end{aligned} \tag{4.4}$$

Similarly, the subsequent components can be computed analogously, yielding the κ-th term approximation:

$$\begin{aligned}
\phi(x,t) \simeq \sum_{n=0}^{\kappa}\phi_n(x,t) =& \frac{\gamma-2k^2}{3} - 2k^2 tanh^2(kx)\\
&+ \frac{\gamma k^3\Gamma(\theta)\tanh(kx)\mathrm{sech}^2(kx)\left((4\theta-4)\Gamma(\theta+1)-4\theta t^{\theta}\right)}{((\theta-1)\Gamma(\theta)-\theta)\Gamma(\theta+1)} + ...
\end{aligned} \tag{4.5}$$

$$\begin{aligned}
\psi(x,t) \simeq \sum_{n=0}^{\kappa}\psi_n(x,t) =& \frac{-4k^2c_0(\gamma+k^2)}{3c_1^2} + \frac{4k^2(\gamma+k^2)}{3c_1}tanh(kx)\\
&+ \frac{4\gamma k^3\left(\gamma+k^2\right)\mathrm{sech}^2(kx)\left(-\theta\Gamma(\theta)+\Gamma(\theta)+t^{\theta}\right)}{3c_1(\theta-\theta\Gamma(\theta)+\Gamma(\theta))} + ...
\end{aligned} \tag{4.6}$$

$$\varphi(x,t) \simeq \sum_{n=0}^{\kappa}\varphi_n(x,t) = c_0 + c_1 tanh(kx) + \frac{\gamma c_1 k\mathrm{sech}^2(kx)\left(-\theta\Gamma(\theta)+\Gamma(\theta)+t^{\theta}\right)}{\theta-\theta\Gamma(\theta)+\Gamma(\theta)} + ... \tag{4.7}$$

Solution using the LVIM

Building upon the theoretical framework developed earlier, the initial iterative solutions are attained as:

$$\begin{aligned}
\phi_0(x,t) &= \frac{\gamma-2k^2}{3} - 2k^2 tanh^2(kx),\\
\psi_0(x,t) &= \frac{-4k^2c_0(\gamma+k^2)}{3c_1^2} + \frac{4k^2(\gamma+k^2)}{3c_1}tanh(kx),\\
\varphi_0(x,t) &= c_0 + c_1 tanh(kx),
\end{aligned} \tag{4.8}$$

and

$$\begin{aligned}
\phi_1(x,t) &= \frac{1}{3}\Big(\gamma + \frac{\gamma k^3\Gamma(\theta)\tanh(kx)\mathrm{sech}^2(kx)\left((12\theta-12)\Gamma(\theta+1)-12\theta t^{\theta}\right)}{((\theta-1)\Gamma(\theta)-\theta)\Gamma(\theta+1)}\\
&\quad + 6k^2\tanh^2(kx) - 2k^2\Big),\\
\psi_1(x,t) &= \frac{4k^2\left(\gamma+k^2\right)\left(c_1\left(\frac{\gamma k\mathrm{sech}^2(kx)\left(-\theta\Gamma(\theta)+\Gamma(\theta)+t^{\theta}\right)}{\theta-\theta\Gamma(\alpha)+\Gamma(\theta)}+\tanh(kx)\right)-c_0\right)}{3c_1^2},\\
\varphi_1(x,t) &= c_1\left(\frac{\gamma k\mathrm{sech}^2(kx)\left(-\theta\Gamma(\theta)+\Gamma(\theta)+t^{\theta}\right)}{\theta-\theta\Gamma(\theta)+\Gamma(\theta)}+\tanh(kx)\right)+c_0,
\end{aligned} \tag{4.9}$$

and so on. The subsequent approximated components can be easily computed by using Eq (3.15).

4.2. Second initial condition

To validate the correctness and reliability of the developed methods when applied to the fractional GHS-KdV system Eq (1.1), we consider another initial condition as follows:

$$\begin{aligned}
\phi(x,0) &= \frac{\gamma - 8k^2}{3} + 4k^2 \tanh^2(kx),\\
\psi(x,0) &= \frac{4k^2 \tanh^2(kx)}{c_1} - \frac{4\left(3c_0k^4 + 4c_1k^4 - 2\gamma c_1k^2\right)}{3c_1^2},\\
\varphi(x,0) &= c_0 + c_1 \tanh^2(kx).
\end{aligned} \tag{4.10}$$

This specific initial condition is important when studying the fractional generalized Hirota-Satsuma (GHS) coupled Korteweg-de Vries (KdV) system because it is carefully chosen to represent a solitary wave profile and to ensure the physical and mathematical consistency of the model. It is noteworthy that [37] presented the exact solution for the GHS-KdV system Eq (1.1) with $\theta = 1$ under the initial condition (4.10) as:

$$\begin{aligned}
\phi(x,t) &= \frac{1}{3}\left(\gamma - 8k^2\right) + 4k^2 \tanh^2(k(\gamma t + x)),\\
\psi(x,t) &= \frac{\left(4k^2\right)\tanh^2(k(\gamma t + x))}{c_1} - \frac{4\left(3c_0k^4 + 4c_1k^4 - 2\gamma c_1k^2\right)}{3c_1^2}\\
\varphi(x,t) &= c_1 \tanh^2(k(\gamma t + x)) + c_0.
\end{aligned} \tag{4.11}$$

Solution using the LADM

By applying the procedure described in the previous section, the initial terms of the LADM are given as

$$\begin{aligned}
\phi_0(x,0) &= \frac{\gamma - 8k^2}{3} + 4k^2 tanh^2(kx),\\
\psi_0(x,0) &= \frac{\left(4k^2\right)\tanh^2(kx)}{c_1} - \frac{4\left(3c_0k^4 + 4c_1k^4 - 2\gamma c_1k^2\right)}{3c_1^2},\\
\varphi_0(x,0) &= c_0 + c_1 tanh^2(kx),
\end{aligned} \tag{4.12}$$

and

$$\begin{aligned}
\phi_1(x,t) &= \frac{1}{c_1((\theta-1)\Gamma(\theta)-\theta)\Gamma(\theta+1)}\Bigg(k^3\Gamma(\theta)\tanh(kx)\,\mathrm{sech}^2(kx)\Big[\theta t^\theta(c_1((48-48k^2)\mathrm{sech}^2(kx)\\
&\quad - 8\gamma + 48k^2 - 48) + c_0(24k^2 - 24)) + \Gamma(\theta+1)(c_0(24k^2 - 24\theta k^2 + 24\theta - 24)\\
&\quad + c_1(48k^2 - 48\theta k^2 + 8\theta\gamma - 8\gamma + (-48\theta + (48\theta - 48)k^2 + 48)\mathrm{sech}^2(kx) - 48))\Big]\Bigg),\\
\psi_1(x,t) &= \frac{8\gamma k^3\Gamma(\theta)\tanh(kx)\,\mathrm{sech}^2(kx)\left(\theta t^\theta - (\theta-1)\Gamma(\theta+1)\right)}{c_1\left(\theta - \theta\Gamma(\theta) + \Gamma(\theta)\right)\Gamma(\theta+1)},\\
\varphi_1(x,t) &= \frac{2\gamma c_1 k\Gamma(\theta)\tanh(kx)\,\mathrm{sech}^2(kx)\left(\theta t^\theta - (\theta-1)\Gamma(\theta+1)\right)}{\left(\theta - \theta\Gamma(\theta) + \Gamma(\theta)\right)\Gamma(\theta+1)}.
\end{aligned} \tag{4.13}$$

Likewise, the remaining components can be easily computed, facilitating the approximation of the solution for the κ-*th* term approximation as:

$$\phi(x,t) \simeq \sum_{n=0}^{\kappa} \phi_n(x,t), \quad \psi(x,t) \simeq \sum_{n=0}^{\kappa} \psi_n(x,t), \quad and \quad \psi(x,t) \simeq \sum_{n=0}^{\kappa} \psi_n(x,t). \tag{4.14}$$

Solution using the LVIM

Applying the procedure detailed earlier, the first iterative solutions are calculated as follows:

$$\begin{aligned} \phi_0(x,0) &= \frac{\gamma - 8k^2}{3} + 4k^2 tanh^2(kx), \\ \psi_0(x,0) &= \frac{\left(4k^2\right)\tanh^2(kx)}{c_1} - \frac{4\left(3c_0k^4 + 4c_1k^4 - 2\gamma c_1k^2\right)}{3c_1^2}, \\ \varphi_0(x,0) &= c_0 + c_1 tanh^2(kx), \end{aligned} \tag{4.15}$$

and

$$\begin{aligned} \phi_1(x,t) = {} & \frac{1}{3}(\gamma - 8k^2) + 4k^2\tanh^2(kx) + \frac{k^3\tanh(kx)\,\mathrm{sech}^2(kx)}{c_1(-\theta + \frac{\theta}{\Gamma(\theta)} + 1)\Gamma(\theta+1)}\Big[c_0\Big(\theta(24 - 24k^2)\,t^\theta \\ & + \Gamma(\theta+1)(-24\theta + (24\theta - 24)k^2 + 24)\Big) \\ & + c_1\Big(\theta t^\theta((48 - 80k^2)\tanh^2(kx) + 8\gamma - 32k^2\mathrm{sech}^2(kx) + 32k^2) \\ & \quad + \Gamma(\theta+1)(-8\theta\gamma + 8\gamma - 32\theta k^2 + (-48\theta + (80\theta - 80)k^2 + 48)\tanh^2(kx) \\ & \quad\quad + (32\theta - 32)k^2\mathrm{sech}^2(kx) + 32k^2)\Big)\Big], \\ \psi_1(x,t) = {} & \frac{8\gamma k^3\tanh(kx)\mathrm{sech}^2(kx)(\theta t^\theta - (\theta-1)\Gamma(\theta+1))}{c_1(-\theta + \frac{\theta}{\Gamma(\theta)} + 1)\Gamma(\theta+1)} \\ & + \frac{4k^2\tanh^2(kx)}{c_1} - \frac{4(3c_0k^4 + 4c_1k^4 - 2\gamma c_1k^2)}{3c_1^2}, \\ \varphi_1(x,t) = {} & \frac{2\gamma c_1 k\,\tanh(kx)\mathrm{sech}^2(kx)(\theta t^\theta - (\theta-1)\Gamma(\theta+1))}{(-\theta + \frac{\theta}{\Gamma(\theta)} + 1)\Gamma(\theta+1)} + c_1\tanh^2(kx) + c_0, \end{aligned} \tag{4.16}$$

and so on.

The subsequent κ-*th* approximations can be straightforwardly determined using Eq (3.15).

5. Numerical results

Here, we will showcase the effectiveness of the suggested methods for handling the fractional GHS-KdV system Eq (1.1) by presenting various graphical representations of the numerical results and comparing our findings with published results from the literature through tabular data. All computations were performed on a laptop running Mathematica 11.2, with 8.00 GB of RAM and a processor; 13th Gen Intel(R) Core(TM) i5-13420H 2.10 GHz processor. The results were computed

using of the absolute errors (AEs), relative absolute errors (RAEs) and the maximum absolute error (MAE) between the exact solution $\sqcap(x,t)$, and the κ-th iteration of the approximate solution $\sqcap_\kappa(x,t)$, which are defined, respectively, as follows:

$$\text{AEs} = |\sqcap(x,t) - \sqcap_\kappa(x,t)|, \tag{5.1}$$

$$RAEs = \frac{|\sqcap(x,t) - u_k(x,t)|}{\sqcap(x,t)}, \tag{5.2}$$

and

$$\text{MAE} = \max_{(x,t)\in[A,B]\times[0,L]} |\sqcap(x,t) - \sqcap_\kappa(x,t)|. \tag{5.3}$$

Suppose that $\phi(x,t)$, $\psi(x,t)$, *and* $\varphi(x,t)$ are defined over the spatial interval $A \le x \le B$ and temporal interval $0 \le t \le L$. A uniform discretization of the domain is constructed via grid points (x_i, t_n) with spatial spacing $h = \triangle x = \frac{B-A}{M}$ and temporal spacing $k = \triangle t = \frac{L}{K}$ where
$x_i = A + ih$ $(i = 0, 1, 2, \cdots, M)$, and $t_n = nk$, $(n = 0, 1, 2, \cdots, K)$.

Numerical analysis under the first initial condition

The numerical outcomes for the AB- fractional GHS-coupled KdV system Eq (1.1) under the initial condition Eq (4.1) are summarized in Tables 2 and 3 visually represented in Figures 1–6 at $k = 0.1, c_1 = 0.1, c_0 = 3/2, \gamma = 3/2$, while the results in Table 4 are tabulated at $k = 0.1, c_1 = 1, c_0 = 1, \gamma = 1$.

Table 2. Comparisons of the AEs and RAEs of $\phi(x,t)$, $\psi(x,t)$, $\varphi(x,t)$ at $x = 0.1$ with the LRPSM [18].

	t	LADM		LVIM		LRPSM [18]	
		AEs (φ)	RAEs (φ)	AEs (φ)	RAEs (φ)	AEs (φ)	RAEs (φ)
$\phi(x,t)$	0.00	0.0	0.0	0.0	0.0	0.0	0.0
	0.02	1.079×10^{-12}	2.187×10^{-12}	5.632×10^{-13}	1.142×10^{-12}	3.807×10^{-5}	7.541×10^{-5}
	0.04	1.726×10^{-11}	3.499×10^{-11}	9.010×10^{-12}	1.826×10^{-11}	7.625×10^{-5}	1.511×10^{-4}
	0.06	8.737×10^{-11}	1.771×10^{-10}	4.560×10^{-11}	9.249×10^{-11}	1.145×10^{-4}	2.269×10^{-4}
	0.08	2.761×10^{-10}	5.597×10^{-10}	1.441×10^{-10}	2.921×10^{-10}	1.529×10^{-4}	3.129×10^{-4}
	0.10	6.740×10^{-10}	6.740×10^{-9}	3.517×10^{-10}	7.130×10^{-10}	1.914×10^{-4}	3.792×10^{-4}
$\psi(x,t)$	0.00	0.0	0.0	0.0	0.0	0.0	0.0
	0.02	1.155×10^{-13}	-3.827×10^{-14}	1.319×10^{-13}	-4.371×10^{-14}	1.679×10^{-5}	5.228×10^{-3}
	0.04	1.948×10^{-12}	-6.457×10^{-13}	2.220×10^{-12}	-7.358×10^{-13}	3.365×10^{-5}	1.042×10^{-2}
	0.06	1.039×10^{-11}	-3.444×10^{-12}	1.179×10^{-11}	-3.910×10^{-12}	5.059×10^{-5}	1.559×10^{-2}
	0.08	3.450×10^{-11}	-1.144×10^{-11}	3.904×10^{-11}	-1.295×10^{-11}	6.761×10^{-5}	2.072×10^{-2}
	0.10	8.829×10^{-11}	8.829×10^{-11}	9.963×10^{-11}	-3.305×10^{-11}	8.470×10^{-5}	2.582×10^{-2}
$\varphi(x,t)$	0.00	0.0	0.0	0.0	0.0	0.0	0.0
	0.02	5.729×10^{-14}	3.816×10^{-14}	6.550×10^{-14}	4.363×10^{-14}	1.880×10^{-3}	7.338×10^{-4}
	0.04	9.672×10^{-13}	6.441×10^{-13}	1.102×10^{-12}	7.342×10^{-13}	3.767×10^{-3}	3.428×10^{-3}
	0.06	5.159×10^{-12}	3.435×10^{-12}	5.858×10^{-12}	3.900×10^{-12}	5.663×10^{-3}	2.348×10^{-3}
	0.08	1.713×10^{-11}	1.141×10^{-11}	1.939×10^{-11}	1.291×10^{-11}	7.568×10^{-3}	7.568×10^{-3}
	0.10	4.385×10^{-11}	2.919×10^{-11}	4.947×10^{-11}	3.294×10^{-11}	9.483×10^{-3}	3.633×10^{-3}

Table 3. Comparison of the MAEs and CPU time of the LADM and LVIM for Eq (1.1) under Eq (4.1) for $-1 \leq x \leq 1,\ 0 \leq t \leq 1$.

κ	LADM				LVIM			
	MAE(ϕ)	MAE(ψ)	MAE(φ)	CPU	MAE(ϕ)	MAE(ψ)	MAE(φ)	CPU
3	6.716×10^{-6}	8.378×10^{-6}	4.161×10^{-6}	0.34375	3.473×10^{-6}	9.444×10^{-6}	4.691×10^{-6}	1.73438
4	3.962×10^{-7}	2.031×10^{-6}	1.009×10^{-6}	0.703125	1.294×10^{-7}	2.550×10^{-6}	1.267×10^{-6}	23.9219
5	8.563×10^{-8}	9.740×10^{-8}	4.802×10^{-8}	1.20313	3.941×10^{-8}	1.685×10^{-7}	8.370×10^{-8}	841.844

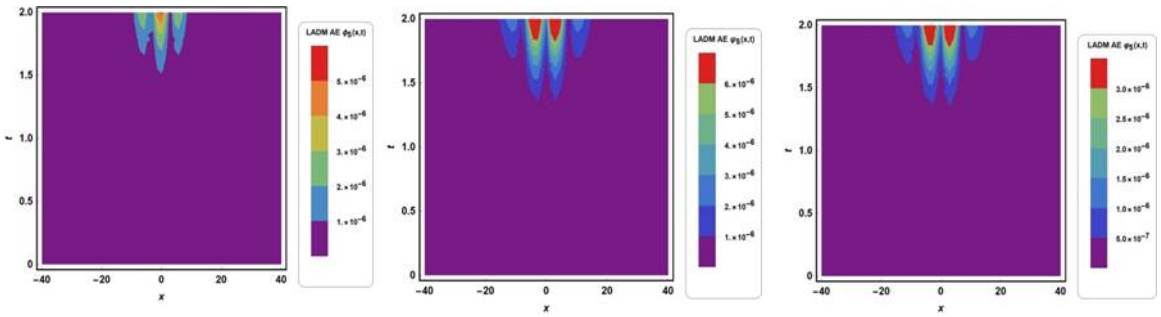

Figure 1. Contour plots of the absolute errors between the exact and LADM solutions of Eq (1.1) under Eq (4.1).

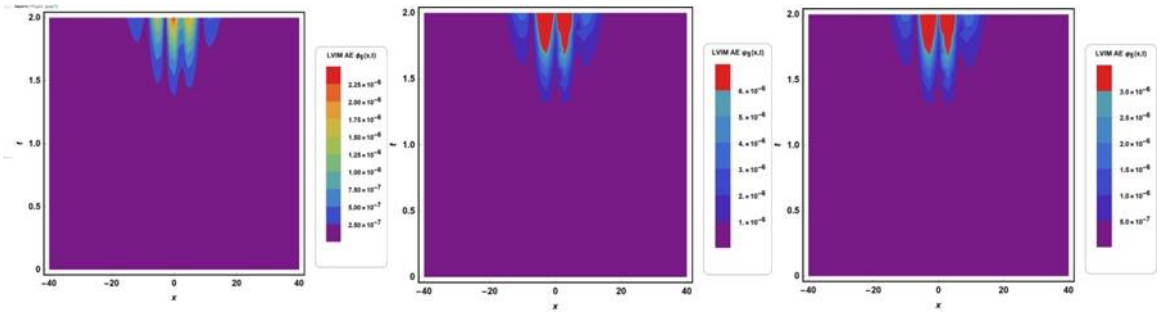

Figure 2. Contour plots of the absolute errors between the exact and LVIM solutions of Eq (1.1) under Eq (4.1).

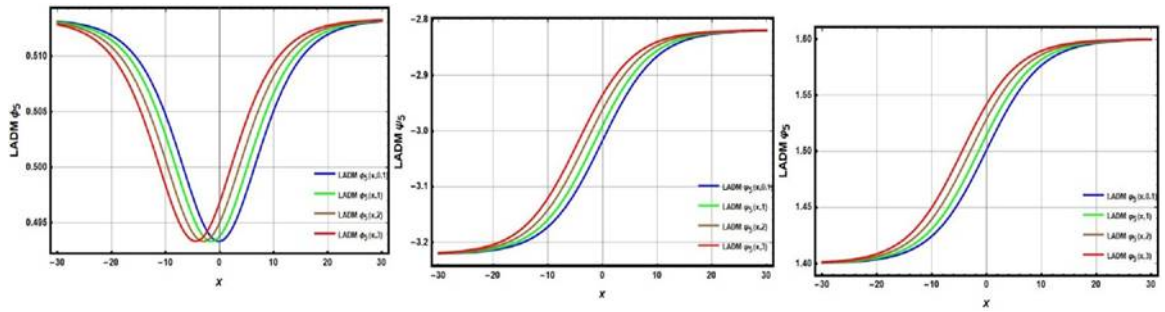

Figure 3. Plots of the LADM solutions at different time levels ($t = 0.1,\ 1,\ 2,\ 3$) of Eq (1.1) under Eq (4.1).

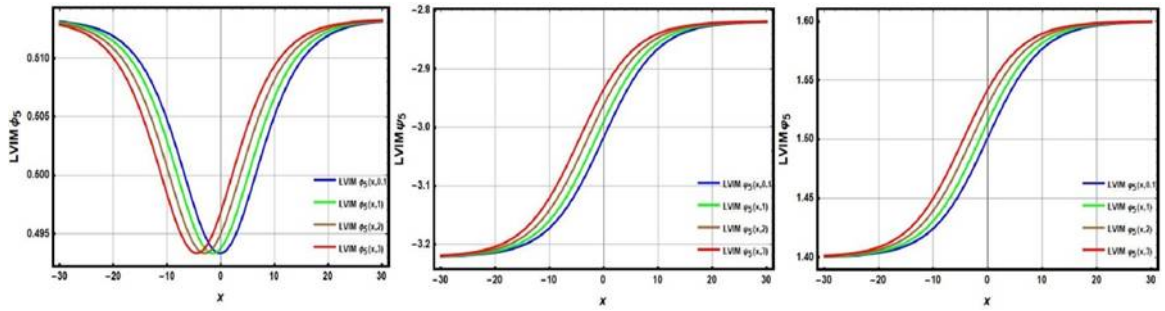

Figure 4. Plots of the LVIM solutions at different time levels ($t = 0.1,\ 1,\ 2,\ 3$) of Eq (1.1) under Eq (4.1).

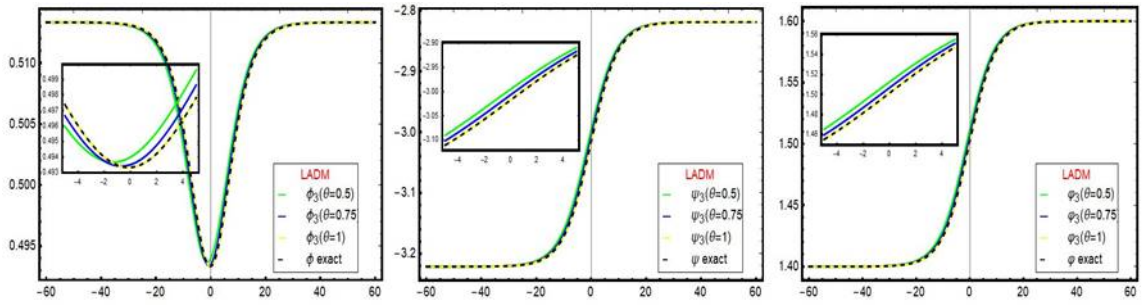

Figure 5. Plots of the LADM solutions at different values of $\theta; \theta = 0.5,\ 0.75,\ 1$ with ESs of Eq (1.1) under Eq (4.1).

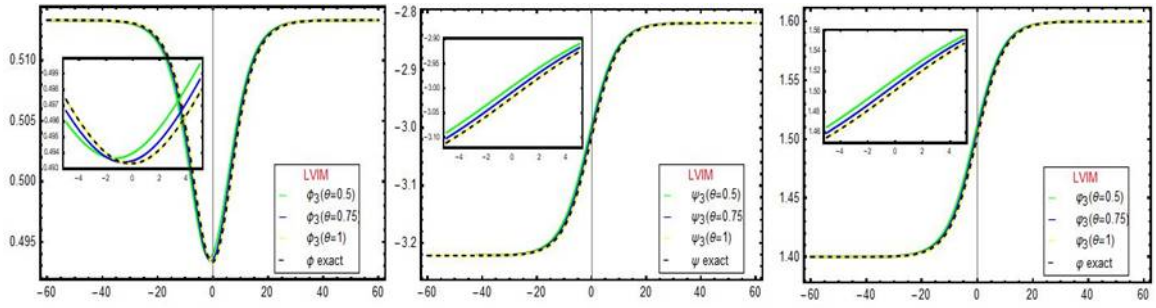

Figure 6. Plots of the LVIM solutions at different values of θ; $\theta = 0.5,\ 0.75,\ 1$ with ESs of Eq (1.1) under Eq (4.1).

Tables 2 and 3 provides detailed comparisons of the absolute errors and relative absolute errors between the two proposed methods LADM and LVIM using the third series approximation with the LRPSM [18] for the functions $\phi(x,t)$, $\psi(x,t)$, and $\varphi(x,t)$ using 6th approximate of the LRPSM solution, respectively. These comparisons are conducted at $x = 0.1$ and over the time interval $t \in [0, 0.1]$. The numerical results clearly demonstrate that the LADM and LVIM converge significantly faster to the exact solution than the RPSM. This faster convergence reflects the strength of the proposed Laplace-based approaches in efficiently handling the non-linearity and memory effects of the fractional system.

Numerical comparisons of the MAEs for $\phi(x,t)$, $\psi(x,t)$, and $\varphi(x,t)$ obtained using the LADM and LVIM are presented in Table 3. The computations are performed over the domains $-1 \leq x \leq 1$ and $0 \leq t \leq 1$ for $\kappa = 3, 4, 5$, where κ represents the number of series terms in the LADM and the number of iterations in the LVIM. The results clearly indicate that increasing κ improves the accuracy of both methods, demonstrating their strong iterative refinement capability. Furthermore, the numerical values produced by the LADM and LVIM exhibit excellent agreement, confirming the consistency and reliability of these techniques for solving the fractional GHS-KdV system. The corresponding CPU times for the LADM and LVIM at different iteration levels ($\kappa = 3, 4, 5$) are also reported in the table. The results show that the LADM outperforms the LVIM in terms of computational speed, highlighting its efficiency and suitability for this class of fractional problems.

To validate the accuracy of the used methods over a large interval, numerical comparisons of AEs for the second approximation of $\phi(x,t)$, $\psi(x,t)$, and $\varphi(x,t)$ obtained using our approaches are presented in Table 4 at $\theta = 1$. These comparisons are conducted for $x \in [-50, 50]$ at $t = 2$ and benchmarked against the second approximate solution of the method in [7]. Our computational findings demonstrate the efficiency of the proposed approaches as well as the approach in [7]. The comprehensive analysis in these tables highlights the advantages of the LADM and LVIM in achieving high accuracy.

Table 4. Comparison of AEs of the 2nd approximation of $\phi(x,t)$, $\psi(x,t)$ and $\varphi(x,t)$ of Eq (1.1) under Eq (4.1) obtained by the LADM and LVIM for $-50 \leqslant x \leqslant 50$, and $t = 2$ with the method in [7] at $k = 0.1, c_1 = 1, c_0 = 1, \gamma = 1$.

x	$\phi(x,t)$			$\psi(x,t)$			$\varphi(x,t)$		
	LADM	LVIM	[7]	LADM	LVIM	[7]	LADM	LVIM	[7]
−50	4.291×10^{-8}	4.2925×10^{-8}	2.49504×10^{-7}	1.4453×10^{-8}	1.4453×10^{-8}	1.18327×10^{-8}	1.35789×10^{-6}	1.07327×10^{-6}	8.78668×10^{-7}
−40	3.154×10^{-7}	3.1617×10^{-7}	1.83949×10^{-6}	1.065×10^{-7}	1.0653×10^{-7}	8.72611×10^{-8}	1.00081×10^{-3}	7.9109×10^{-6}	6.47979×10^{-6}
−30	2.2425×10^{-6}	2.2818×10^{-6}	1.33693×10^{-5}	7.721×10^{-7}	7.7295×10^{-7}	6.35469×10^{-7}	7.25779×10^{-5}	5.7397×10^{-5}	4.71883×10^{-5}
−20	1.221×10^{-5}	1.41781×10^{-5}	8.72541×10^{-5}	4.94265×10^{-6}	4.9826×10^{-6}	4.211×10^{-6}	4.6633×10^{-4}	3.699×10^{-4}	3.12728×10^{-4}
−10	2.583×10^{-5}	3.07801×10^{-5}	2.14213×10^{-4}	1.0349×10^{-5}	1.1231×10^{-5}	1.2457×10^{-5}	1.0686×10^{-3}	8.339×10^{-4}	9.25057×10^{-4}
0	2.085×10^{-5}	2.08597×10^{-5}	8.1114×10^{-4}	3.53457×10^{-5}	35345×10^{-5}	3.53457×10^{-5}	2.62468×10^{-3}	2.624×10^{-3}	2.62468×10^{-3}
10	1106×10^{-5}	455518×10^{-5}	2.90545×10^{-4}	1.1575×10^{-5}	124574×10^{-5}	1.12311×10^{-5}	55983×10^{-4}	9.2505×10^{-4}	8.33992×10^{-4}
20	10696×10^{-5}	1266×10^{-5}	1.14092×10^{-4}	4.17142×10^{-6}	4.2114×10^{-6}	4.98263×10^{-6}	2.1045×10^{-4}	3.12728×10^{-4}	3.69997×10^{-4}
30	1.8508×10^{-6}	1.89015×10^{-6}	1.75413×10^{-5}	6.346×10^{-7}	6.354×10^{-7}	7.72958×10^{-7}	3.1884×10^{-5}	4.71883×10^{-5}	5.73978×10^{-5}
40	2.585×10^{-7}	2.5923×10^{-7}	2.4149×10^{-6}	8.7245×10^{-8}	8.7261×10^{-8}	1.06534×10^{-6}	4.3802×10^{-6}	6.47979×10^{-6}	7.91091×10^{-6}
50	3.5134×10^{-8}	3.51476×10^{-8}	3.27577×10^{-7}	1.18324×10^{-8}	1.1832×10^{-8}	1.44533×10^{-8}	5.9400×10^{-7}	8.78668×10^{-7}	1.07327×10^{-6}

To verify the performance and accuracy of our methods for solving Eq (1.1) under the first initial condition Eq (4.1), a series of graphical representations are provided. The contour plots of the absolute errors for $\phi(x,t)$, $\psi(x,t)$, and $\varphi(x,t)$ using the LADM and LVIM are shown in Figures 1 and 2, respectively, over $x \in [-40, 40]$, and $t \in [0, 2]$. These plots highlight the minimal errors and confirm the high precision of both methods in solving the fractional system. Figures 3 and 4 further illustrate the applicability of the LADM and LVIM in obtaining approximate solutions for $\phi(x,t)$, $\psi(x,t)$, and $\varphi(x,t)$ at different time levels ($t = 0.1,\ 1,\ 2,\ 3$). These graphs reveal the robustness of the proposed methods in capturing the dynamics of the system over varying temporal and spatial domains. Additionally, Figures 5 and 6 evaluate the performance of the LADM using just four terms and the third approximation of the LVIM for deriving solutions at various fractional orders. The solutions are analyzed for $x \in [-60, 60]$ with fractional orders $\theta = 0.5, 0.75, 1$, alongside the exact solutions. These figures demonstrate that as the fractional order approaches an integer, the approximate solutions increasingly converge to the exact solution.

Numerical analysis of the fractional GHS-KdV system under the second initial condition

The computational findings of the fractional GHS-KdV coupled system Eq (1.1) under Eq (4.10) obtained using the LADM and LVIM are presented in Tables 5 and 6, while their graphical representations are illustrated in Figures 7–10. Table 5 provides a numerical comparison of the absolute errors between the second approximation of our findings using the LADM and LVIM with those reported in [7] when $\theta = 1$ for $x \in [-50, 50]$, $t = 1$ for $k = 0.1, c_1 = c_0 = \gamma = 1$. Table 6 tabulates a comparison of the absolute errors at discrete points of x *and* t for the parameters $k = 0.1, c_1 = c_0 = \gamma = 3/2$, against the results of [38] . Figures 7 and 8 depict the space time surface plots of the exact, and approximate solutions obtained via the LADM and LVIM, respectively. The numerical finding of LADM and LVIM for the functions $\phi(x,t)$, $\psi(x,t), \varphi(x,t)$ are displayed for different values of the fractional parameter θ are plotted in Figures 9 and 10; respectively.

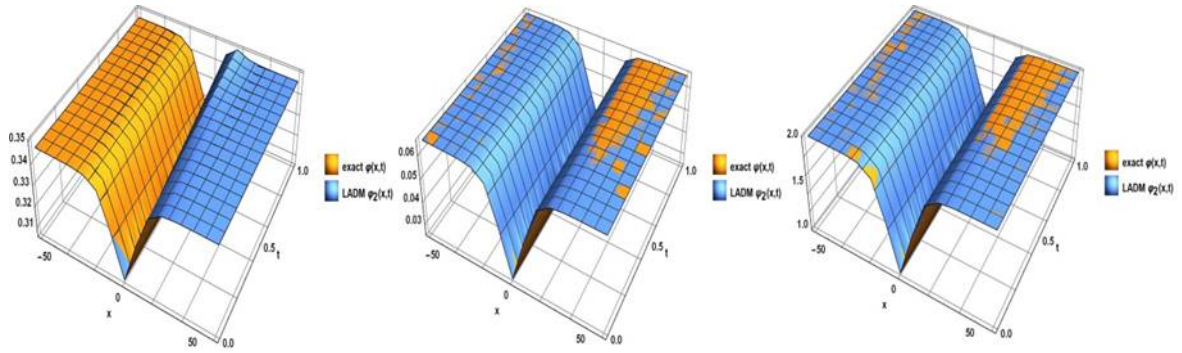

Figure 7. The surfaces of the exact and LADM solutions for Eq (1.1) under Eq (4.10).

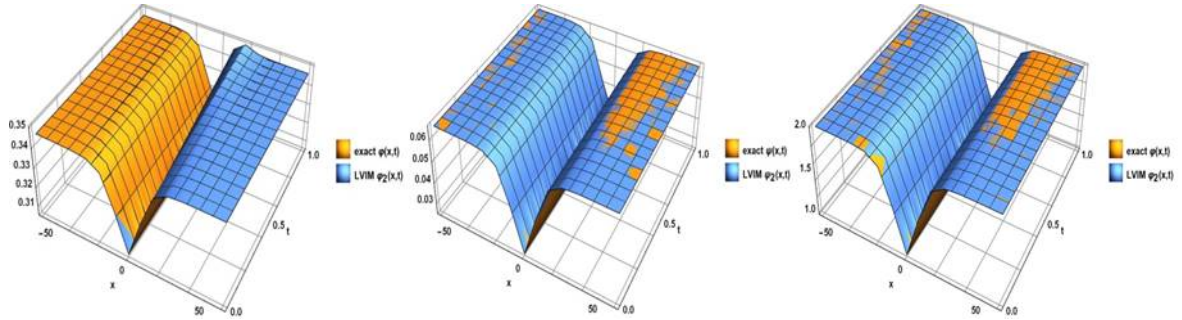

Figure 8. The surfaces of the exact and LVIM solutions for Eq (1.1) under Eq (4.10).

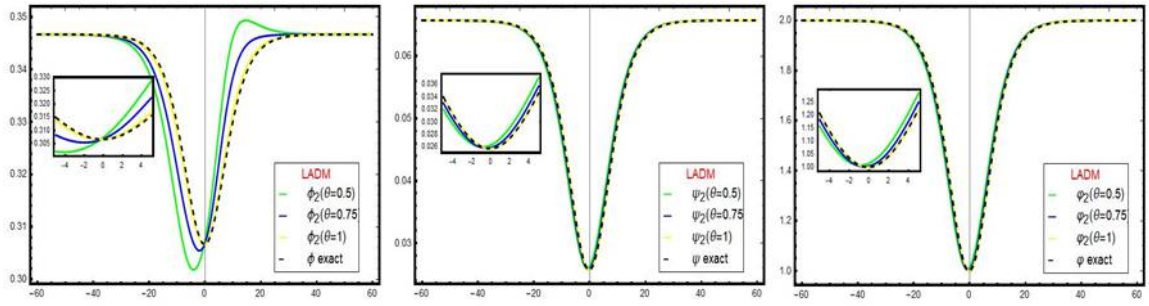

Figure 9. Plots of the LADM solutions at different values of $\theta; \theta = 0.5,\ 0.75,\ 1$ with the exact solutions of Eq (1.1) under Eq (4.10).

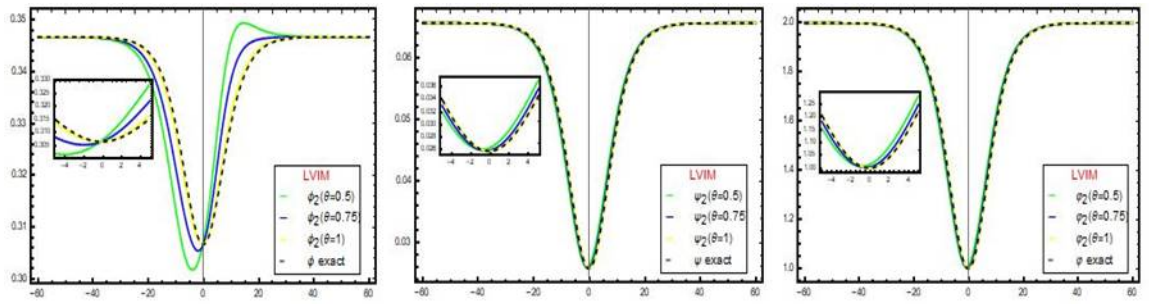

Figure 10. Plots of the LVIM solutions at different values of $\theta; \theta = 0.5,\ 0.75,\ 1$ with the exact solutions Eq (1.1) under Eq (4.10).

Table 5. Comparison of AEs of the 2nd approximation of $\phi(x,t)$, $\psi(x,t)$, and $\varphi(x,t)$ of Eq (1.1) under Eq (4.10) obtained by our proposed methods for $-50 \leqslant x \leqslant 50$ and $t = 1$ with the method in [7] at $k = 0.1, c_1 = 1, c_0 = 1, \gamma = 1$.

x	$\phi(x,t)$			$\psi(x,t)$			$\varphi(x,t)$		
	LADM	LVIM	[7]	LADM	LVIM	[7]	LADM	LVIM	[7]
−50	1.2904×10^{-5}	$129 * \times 10^{-5}$	1.374×10^{-6}	1.021×10^{-8}	1.021×10^{-8}	9.198×10^{-9}	2.552×10^{-7}	2.554×10^{-7}	2.297×10^{-7}
−40	9.516×10^{-5}	952×10^{-5}	1.013×10^{-5}	7.640×10^{-8}	7.663×10^{-8}	6.691×10^{-8}	1.910×10^{-6}	1.916×10^{-6}	1.662×10^{-6}
−30	6.933×10^{-4}	6.933×10^{-4}	7.38904×10^{-5}	6.739×10^{-6}	6.273×10^{-7}	4.386×10^{-7}	154×10^{-5}	1.568×10^{-5}	1.037×10^{-5}
−20	4.616×10^{-3}	4.618×10^{-3}	4.990×10^{-5}	5.760×10^{-5}	4.989×10^{-6}	6.682×10^{-7}	1.684×10^{-4}	1.816×10^{-4}	1.227×10^{-5}
−10	1.645×10^{-2}	1.644×10^{-2}	2.386×10^{-3}	1.035×10^{-5}	6.232×10^{-5}	3.457×10^{-5}	1.440×10^{-3}	1.556×10^{-3}	1.546×10^{-3}
0	1.215×10^{-4}	1.214×10^{-4}	3.818×10^{-4}	2.652×10^{-6}	2.652×10^{-6}	2.652×10^{-6}	6.629×10^{-5}	6.629×10^{-5}	6.629×10^{-5}
10	1.638×10^{-2}	1.637×10^{-2}	2.784×10^{-3}	6.560×10^{-5}	6.184×10^{-5}	3.126×10^{-5}	1.664×10^{-3}	1.546×10^{-3}	1.558×10^{-3}
20	4.630×10^{-3}	4.632×10^{-3}	5.886×10^{-4}	1.013×10^{-6}	4.909×10^{-7}	5.776×10^{-6}	2.534×10^{-5}	1.227×10^{-5}	1.816×10^{-4}
30	6.960×10^{-4}	6.961×10^{-4}	8.398×10^{-5}	4.027×10^{-7}	4.147×10^{-7}	5.962×10^{-7}	1.007×10^{-5}	1.037×10^{-5}	1.568×10^{-5}
40	9.556×10^{-5}	9.555×10^{-5}	1.145×10^{-5}	6.624×10^{-8}	6.647×10^{-8}	7.605×10^{-8}	1.656×10^{-6}	1.662×10^{-6}	7.91091×10^{-6}
50	1.30×10^{-5}	1.30×10^{-5}	1.550×10^{-6}	9.185×10^{-9}	9.189×10^{-9}	1.020×10^{-8}	2.30×10^{-7}	2.30×10^{-7}	1.073×10^{-6}

Table 6. Comparison of AEs of the 2nd approximation of $\phi(x,t)$, $\psi(x,t)$, and $\varphi(x,t)$ of Eq (1.1) under Eq (4.10) obtained by the LADM and LVIM for various values of x, and t with the HPM [38] at $k = 0.1, c_1 = 3/2, c_0 = 3/2, \gamma = 3/2$.

(x,t)	$\phi(x,t)$			$\psi(x,t)$			$\varphi(x,t)$		
	LADM	LVIM	HPM [38]	LADM	LVIM	HPM [38]	LADM	LVIM	HPM [38]
(0.1, 0.1)	2.4954×10^{-5}	2.49566×10^{-5}	2.49546×10^{-5}	1.47515×10^{-9}	1.65474×10^{-9}	1.47515×10^{-9}	8.29773×10^{-8}	9.30793×10^{-8}	8.2977×10^{-8}
(0.1, 0.2)	4.87267×10^{-5}	4.87287×10^{-5}	$5.23307E \times 10^{-5}$	2.42843×10^{-9}	2.60717×10^{-9}	1.8217×10^{-8}	1.36599×10^{-7}	1.46653×10^{-7}	1.02473×10^{-6}
(0.1, 0.3)	7.25151×10^{-5}	7.25171×10^{-5}	8.2206×10^{-5}	3.75883×10^{-9}	3.9361×10^{-9}	8.47873×10^{-8}	2.11434×10^{-7}	2.21408×10^{-7}	4.76929×10^{-6}
(0.2, 0.1)	5.23307×10^{-5}	5.2363×10^{-5}	8.2206×10^{-5}	1.82174×10^{-8}	2.10911×10^{-8}	2.4284×10^{-9}	1.02473×10^{-6}	1.18637×10^{-6}	1.36599×10^{-7}
(0.2, 0.2)	9.8964×10^{-5}	9.9928×10^{-5}	9.9896×10^{-5}	2.35342×10^{-8}	2.6394×10^{-8}	2.3534×10^{-8}	1.3238×10^{-6}	1.48468×10^{-6}	1.3238×10^{-6}
(0.2, 0.3)	1.47489×10^{-4}	1.47521×10^{-4}	1.536×10^{-4}	3.03377×10^{-8}	3.31751×10^{-8}	1.0004×10^{-7}	1.7065×10^{-6}	1.8661×10^{-6}	5.6274×10^{-6}
(0.3, 0.1)	8.22061×10^{-5}	8.23695×10^{-5}	7.25151×10^{-5}	8.47873×10^{-8}	9.93364×10^{-8}	3.75883×10^{-9}	4.76929×10^{-6}	5.58767×10^{-6}	2.1143×10^{-7}
(0.3, 0.2)	1.53616×10^{-4}	1.53778×10^{-4}	1.474×10^{-4}	1.00043×10^{-7}	1.14524×10^{-7}	3.0337×10^{-8}	5.62741×10^{-6}	6.44198×10^{-6}	1.70650×10^{-6}
(0.3, 0.3)	2.25057×10^{-4}	2.25219×10^{-4}	2.2505×10^{-4}	1.18568×10^{-7}	1.32935×10^{-7}	1.18568×10^{-7}	6.66945×10^{-6}	7.47758×10^{-6}	1.70650×10^{-6}

6. Conclusions

The present study has systematically explored the application of Laplace-based methodologies to the fractional GHS-KdV system within the AB fractional calculus framework. The use of the AB-CFD operator with a Mittag-Leffler kernel enables accurate modeling of non-singular fading memory and effectively captures both short- and long-term nonlinear wave dynamics. Integrating this operator into the LADM and LVIM required a tailored Laplace domain reformulation, representing a key methodological advancement.

The analysis confirms that both the LADM and LVIM provide robust computational frameworks capable of efficiently handling the inherent non-linearity and memory effects of fractional-order systems without conventional simplifying assumptions. The comparative results reveal strong consistency between the two methods, with excellent agreement of solution profiles. Moreover, the convergence behavior demonstrates that accuracy improves systematically with additional series terms. Also, both methods accurately capture the limiting behavior as the fractional order approaches the classical integer case, ensuring mathematical consistency.

However, certain limitations exist such as sensitivity to exact initial conditions, challenges in Laplace inversion for complex source terms, and potential computational inefficiency in constructing higher-order Adomian polynomials for strongly nonlinear problems.

Overall, the developed framework offers a powerful and flexible approach for analyzing nonlinear fractional systems with memory effects. It can be readily extended to other classes of fractional PDEs and contributes to the advancement of analytical numerical techniques in fractional calculus. Future work will focus on extending the proposed methods to two-dimensional systems and exploring adaptive strategies for improved convergence and efficiency.

Author contributions

Mofida Zaki: Methodology, software, formal analysis, conceptualization, writing—original draft; M. Abdelgaber: Formal analysis, validation, writing—original draft; Hoda F. Ahmed: Methodology, software, formal analysis, conceptualization, validation, review and editing; W. A. Hashem: Methodology, software, formal analysis, validation. All authors have read and agreed to the published version of the manuscript.

Use of Generative-AI tools declaration

The authors declare they have not used Artificial Intelligence (AI) tools in the creation of this article.

Acknowledgments

The authors are thankful to the Deanship of Scientific Research at Najran University for funding this work under the General Research Funding program grant code (NU/EFP/SERC/13/218).

Conflict of interest

The authors declare that there is no conflict of interests regarding the publication of this paper.

References

1. I. Podlubny, *Fractional differential equations: An introduction to fractional derivatives, fractional differential equations, to methods of their solution and some of their applications*, 1999.
2. G. Barbero, L. R. Evangelista, R. S. Zola, E. K. Lenzi, A. M. Scarfone, A brief review of fractional calculus as a tool for applications in physics: Adsorption phenomena and electrical impedance in complex fluids, *Fractal Fract.*, **8** (2024), 369. https://doi.org/10.3390/fractalfract8070369
3. N. S. Alharthi, Efficient simulation of plasma physics' time fractional modified Korteweg-de Vries equations, *PLoS One*, **20** (2025), e0316218. https://doi.org/10.1371/journal.pone.0316218
4. V. T. Hoang, J. Widjaja, Y. L. Qiang, M. K. Liu, T. J. Alexander, A. F. Runge, et al., Nonlinear wave propagation governed by a fractional derivative, *Nat. Commun.*, **16** (2025), 5469. https://doi.org/10.1038/s41467-025-60625-4
5. H. Sun, Y. Zhang, D. Baleanu, W. Chen, Y. Chen, A new collection of real world applications of fractional calculus in science and engineering, *Commun. Nonlinear Sci.*, **64** (2018), 213–231. https://doi.org/10.1016/j.cnsns.2018.04.019
6. Y. Wu, X. Geng, X. Hu, S. Zhu, A generalized Hirota-Satsuma coupled Korteweg-de Vries equation and Miura transformations, *Phys. Lett. A*, **255** (1999), 259–264. https://doi.org/10.1016/S0375-9601(99)00163-2
7. M. Jibran, R. Nawaz, A. Khan, S. Afzal, Iterative solutions of Hirota-Satsuma coupled KdV and modified coupled KdV systems, *Math. Probl. Eng.*, **2018** (2018), 9042039. https://doi.org/10.1155/2018/9042039
8. A. Kumar, R. D. Pankaj, Laplace-modified decomposition method for the generalized Hirota-Satsuma coupled KdV equation, *Can. J. Basic Appl. Sci.*, **3** (2015), 126–133.
9. R. Abazari, M. Abazari, Numerical simulation of generalized Hirota-Satsuma coupled KdV equation by RDTM and comparison with DTM, *Commun. Nonlinear Sci.*, **17** (2012), 619–629. https://doi.org/10.1016/j.cnsns.2011.05.022
10. H. Gundogdu, O. F. Gozukizil, Double Laplace decomposition method and exact solutions of Hirota, Schrödinger and complex mKdV equations, *Konuralp J. Math.*, **7** (2019), 7–15.
11. M. Inc, M. T. Gencoglu, A. Akgül, Application of extended Adomian decomposition method and extended variational iteration method to Hirota-Satsuma coupled KdV equation, *J. Adv. Phys.*, **6** (2017), 216–222. https://doi.org/10.1166/jap.2017.1326
12. O. W. Lawal, A. C. Loyimi, L. M. Erinle-Ibrahim, Algorithm for solving a generalized Hirota-Satsuma coupled KdV equation using homotopy perturbation transform method, *Sci. World J.*, **13** (2018), 23–28. https://doi.org/10.4314/swj.v13i3
13. J. Hristov, On the Atangana-Baleanu derivative and its relation to the fading memory concept: the diffusion equation formulation, In: *Fractional derivatives with Mittag-Leffler kernel: Theory and applications in science and engineering*, Cham: Springer, 2019. https://doi.org/10.1007/978-3-030-11662-0-11

14. A. Atangana, D. Baleanu, New fractional derivatives with nonlocal and non-singular kernel: theory and application to heat transfer model, *Therm. Sci.*, **20** (2016), 763–769. https://doi.org/10.2298/TSCI160111018A

15. I. Abbas, R. Tiwari, A. E. Abouelregal, Atangana-Baleanu fractional approach to photothermal wave propagation in semiconductor materials under the influence of a moving heat source, *Mech. Solids*, **2025** (2025), 1–18. https://doi.org/10.1134/S002565442560240X

16. A. E. Abouelregal, M. Marin, A. Foul, S. S. Askar, Coupled responses of thermomechanical waves in functionally graded viscoelastic nanobeams via thermoelastic heat conduction model including Atangana-Baleanu fractional derivative, *Sci. Rep.*, **14** (2024), 9122. https://doi.org/10.1038/s41598-024-58866-2

17. M. Toufik, A. Atangana, New numerical approximation of fractional derivative with non-local and non-singular kernel: Application to chaotic models, *Eur. Phys. J. Plus*, **132** (2017), 444. https://doi.org/10.1140/epjp/i2017-11717-0

18. R. Saadeh, O. Ala'yed, A. Qazza, Analytical solution of coupled Hirota-Satsuma and KdV equations, *Fractal Fract.*, **6** (2022), 694. https://doi.org/10.3390/fractalfract6120694

19. B. R. Sontakke, A. Shaikh, K. S. Nisar, Approximate solutions of a generalized Hirota-Satsuma coupled KdV and a coupled mKdV systems with time fractional derivatives, *Malaysian J. Math. Sci.*, **12** (2018), 175–196.

20. L. Akinyemi, O. S. Iyiola, A reliable technique to study nonlinear time-fractional coupled Korteweg-de Vries equations, *Adv. Differ. Equ.*, **2020** (2020), 169. https://doi.org/10.1186/s13662-020-02625-w

21. M. H. Heydari, Z. Avazzadeh, C. Cattani, Numerical solution of variable-order space-time fractional KdV-Burgers-Kuramoto equation by discrete Legendre polynomials, *Eng. Comput.*, **38** (2022), 859–869. https://doi.org/10.1007/s00366-020-01181-x

22. M. A. Saker, S. S. Ezz-Eldien, A. H. Bhrawy, A pseudospectral method for solving the time-fractional generalized Hirota-Satsuma coupled KdV equation, *Romanian J. Phys.*, **62** (2017), 105.

23. A. H. Ganie, S. Noor, M. Al Huwayz, A. Shafee, S. A. El-Tantawy, Numerical simulations for fractional Hirota-Satsuma coupled Korteweg-de Vries systems, *Open Phys.*, **22** (2024), 20240008. https://doi.org/10.1515/phys-2024-0008

24. O. J. Algahtani, Investigation of a spatio-temporal fractal fractional coupled Hirota system, *Fractal Fract.*, **8** (2024), 178. https://doi.org/10.3390/fractalfract8030178

25. S. Mahmood, R. Shah, H. Khan, M. Arif, Laplace Adomian decomposition method for multidimensional time-fractional Navier-Stokes equation, *Symmetry*, **11** (2019), 149. https://doi.org/10.3390/sym11020149

26. H. F. Ahmed, M. S. Bahgat, M. Zaki, Numerical approaches to system of fractional partial differential equations, *J. Egypt. Math. Soc.*, **25** (2017), 141–150. https://doi.org/10.1016/j.joems.2016.12.004

27. H. F. Ahmed, M. S. M. Bahgat, M. Zaki, Analytical approaches to space- and time-fractional coupled Burgers' equations, *Pramana J. Phys.*, **92** (2019), 38. https://doi.org/10.1007/s12043-018-1693-z

28. N. Ngarhasta, B. Some, K. Abbaoui, Y. Cherruault, New numerical study of Adomian method applied to a diffusion model, *Kybernetes*, **31** (2002), 61–75. https://doi.org/10.1108/03684920210413764

29. M. M. Al-Sawalha, A. Khan, O. Y. Ababneh, T. Botmart, Fractional view analysis of Kersten-Krasil'shchik coupled KdV-mKdV systems with non-singular kernel derivatives, *AIMS Math.*, **7** (2022), 18334–18359. https://doi.org/10.3934/math.20221010

30. A. Nazneen, R. Nawaz, L. Zada, N. Ali, M. Benghanem, H. Ahmad, Analysis of the non-linear higher dimensional fractional differential equations arising in dusty plasma using the Atangana-Baleanu fractional derivative, *Results Eng.*, **25** (2025), 104116. https://doi.org/10.1016/j.rineng.2025.104116

31. D. Baleanu, H. K. Jassim, H. Ahmed, J. Singh, D. Kumar, R. Shah, et al., A mathematical theoretical study of Atangana-Baleanu fractional Burger's equations, *Partial Differ. Equ. Appl. Math.*, **11** (2024), 100741. https://doi.org/10.1016/j.padiff.2024.100741

32. F. Ogunfiditimi, N. Okiotor, Solution of modified Hirota-Satsuma coupled KdV equations by variational iteration method, *IJMTT*, **67** (2021), 113–125. https://doi.org/10.14445/22315373/IJMTT-V67I5P514

33. A. M. Wazwaz, The variational iteration method: A reliable analytic tool for solving linear and nonlinear wave equations, *Comput. Math. Appl.*, **54** (2007), 926–932. https://doi.org/10.1016/j.camwa.2006.12.038

34. M. Inc, Numerical simulation of KdV and mKdV equations with initial conditions by the variational iteration method, *Chaos Soliton. Fract.*, **34** (2007), 1075–1081. https://doi.org/10.1016/j.chaos.2006.04.069

35. S. Kumar, P. Pandey, Quasi wavelet numerical approach of nonlinear reaction-diffusion and integro reaction-diffusion equation with Atangana-Baleanu time fractional derivative, *Chaos Soliton. Fract.*, **130** (2020), 109456. https://doi.org/10.1016/j.chaos.2019.109456

36. E. F. Doungmo Goufo, S. Kumar, Shallow water wave models with and without singular kernel: existence, uniqueness, and similarities, *Math. Probl. Eng.*, **2017** (2017), 4609834. https://doi.org/10.1155/2017/4609834

37. E. Fan, Soliton solutions for a generalized Hirota-Satsuma coupled KdV equation and a coupled mKdV equation, *Phys. Lett. A*, **282** (2001), 18–22. https://doi.org/10.1016/S0375-9601(01)00161-X

38. D. D. Ganji, M. Rafei, Solitary wave solutions for a generalized Hirota-Satsuma coupled KdV equation by homotopy perturbation method, *Phys. Lett. A*, **356** (2006), 131–137. https://doi.org/10.1016/j.physleta.2006.03.039